ELSEVIER

Journal of Power Sources 112 (2002) 401–409

JOURNAL OF POWER SOURCES

www.elsevier.com/locate/jpowsour

Cyclic voltammetric deposition of hydrous ruthenium oxide for electrochemical supercapacitors: effects of the chloride precursor transformation

Chi-Chang Hu*, Kwang-Huei Chang

Department of Chemical Engineering, National Chung Cheng University, Chia-Yi 621, Taiwan

Received 8 January 2002; received in revised form 1 July 2002; accepted 25 July 2002

Abstract

Ruthenium chloride and iridium chloride precursors (denoted hereafter as $RuCl_3{\cdot}aH_2O$ and $IrCl_3{\cdot}bH_2O$) reacted with water molecules and transformed into the chloro-oxy-hydroxyl-metal (denoted as $Ru(OH)_\delta Cl_{3-\delta}{\cdot}cH_2O$ and $Ir(OH)_\omega Cl_{3-\omega}{\cdot}dH_2O$) structures when they were dissolved in water. The storage time, preheating, and initial pH of the deposition baths were demonstrated to significantly influence the structures of these dissolved precursors. The rate of hydrous oxide deposition by means of cyclic voltammetry was predominantly determined by the structures of the dissolved precursors and the initial pH of the deposition bath, which also caused a variation in the performance (i.e. specific capacitance) of the hydrous oxides (i.e. $RuO_x{\cdot}nH_2O$ and $(Ru + Ir)O_y{\cdot}mH_2O$) for the application of electrochemical supercapacitors.

Keywords: Structural transformation; Hydrous ruthenium–iridium oxides; Cyclic voltammetry; Electrochemical supercapacitor; Pseudocapacitance

1. Introduction

Due to the unique properties of high pulse power density [1,2], electrochemical (EC) supercapacitors have been recognized as an important and effective device promoting the performance of the energy storage and conversion systems. The most promising materials for EC supercapacitors should utilize both the fast and reversible faradaic pseudocapacitance coming from the redox transitions of the interfacial electroactive species [2–9] and the indefinitely reversible capacitance of electric double-layer formed at the electrolyte–electrode interface [9–11]. Based on this point of view, the electrochemical supercapacitors can be considered as a hybrid device exhibiting transitional behavior between batteries and capacitors. Since the capacitance of electrical double-layer is very low (5–30 μF cm^{-2} in usual), potential candidates of electrodes should be consisted of electroactive materials with very high surface areas, which prosecute the fast reversible redox transitions in the potential window of charge and discharge.

Both amorphous and microcrystalline ruthenium oxides [1–4,7–9,12,13] have been employed as the electrode materials for the EC supercapacitors although ruthenium is a noble metal. Moreover, the intercalation of hydrous iridium oxide (denoted as $IrO_z{\cdot}kH_2O$) into the hydrous ruthenium oxide (denoted as $RuO_x{\cdot}nH_2O$) matrix greatly enhanced the utilization of the electroactive species [3,8] while an understanding of the preparation of these hydrous oxides with very high specific capacitance is still very lack. Moreover, the kinetics of electron transfer and/or the diffusion of protons within the electroactive materials determined the reversibility of redox transitions [1–4,7–9,14–16]. An integration relating the electrochemical characteristics and textural properties to their preparation methods are very important in searching and optimizing the suitable materials for the application of EC supercapacitors.

In our previous work [3,4,7,8], $RuO_x{\cdot}nH_2O$ and $(Ru + Ir)O_y{\cdot}mH_2O$, prepared by cyclic voltammetry, were found to exhibit high pseudocapacitance with good electrochemical reversibility in the potential region of water decomposition. The performance and utilization of these materials, however, were found to strongly depend on the deposition conditions [7] that significantly influenced the electrochemical characteristics of hydrous oxides. In addition, the mechanism of hydrous oxide deposition was expected to be a function of the chemical structure of the dissolved precursor [7,8]. Accordingly, the effects of storage time, preheating and initial pH of the precursor solutions on the chemical structures of

* Corresponding author. Tel.: +886-5-2720411x33411; fax: +886-5-2721206.
E-mail address: chmhcc@ccu.edu.tw (C.-C. Hu).

0378-7753/02/$ – see front matter © 2002 Published by Elsevier Science B.V.
PII: S0378-7753(02)00397-X

dissolved $RuCl_3 \cdot aH_2O$ and/or $IrCl_3 \cdot bH_2O$ were systematically investigated. The performance of these oxides in the application of EC supercapacitors was also studied.

2. Experimental

The preparation of $RuO_x \cdot nH_2O$ and $(Ru + Ir)O_y \cdot mH_2O$ films is similar to that outlined in our previous work [3,4,7,8,16]. Prior to voltammetric deposition, commercial 99% titanium substrates (10 mm × 10 mm × 2 mm) were mechanically polished by emery particles blown by a high-pressure air compressor. These substrates were then degreased with soap and water, and etched in a 6 M HCl solution at ca. 90 °C for 1.5 h. They were rinsed with water again, and then pickled for 10 min in a solution containing *N*,*N*-dimethylformamide (DMF, Wako E.P., Japan), water, and HF (Wako E.P., Japan) with volumes of 40, 7.5, and 2.5 cm^3, respectively. After pickling, the substrates were rinsed with acetone and water, coated with PTFE films, and then placed in the plating solution. The exposed surface area of these substrates is equal to 1 cm^2. The plating baths are mainly consisted of 0.1 M KCl and 5 mM $RuCl_3 \cdot aH_2O$ (Johnson Matthey). For binary oxides, 1 mM $IrCl_3 \cdot bH_2O$ (Johnson Matthey) was added into the plating baths. Note that some deposition solutions have been subjected to certain pretreatments (e.g. stored in a flask from 0 to 144 h or preheating at 60 or 80 °C for 20 min). Finally, the initial pH of the deposition solutions was adjusted to the specified value with 1 M HCl or 1 M NaOH before the electrochemical deposition. The hydrous oxide-coated electrodes were prepared by electrolytic deposition through means of cyclic voltammetry between −200 and 1000 mV at 50 mV s^{-1} for 120 cycles. After deposition, the PTFE films were removed from the electrodes. These electrodes before and after oxide deposition were dried by a cool airflow. The loading of oxides was confirmed by the weight difference of electrodes before and after oxide deposition. The hydrous oxide-coated electrodes with exposed geometric surface areas of 1 cm^2 for the electrochemical measurement were doubly coated with epoxy resin and PTFE films.

Cyclic voltammetry for the deposition and characterization of $RuO_x \cdot nH_2O$ and $(Ru + Ir)O_y \cdot mH_2O$ films was performed by an electrochemical analyzer system, CHI 633A (CH Instrument Inc., USA). All experiments were carried out in a three-compartment cell. An Ag/AgCl electrode (Argenthal, 3 M KCl, 207 mV versus SHE at 25 °C) was used as the reference electrode meanwhile a piece of Pt gauze with an exposed area of 5 cm^2 was employed as the counter electrode. A Luggin capillary, whose tip was set at a distance of 1–2 mm from the surface of the working electrode, was used to minimize errors due to *iR* drop in the electrolytes. The scan rate of CV was kept at 20 mV s^{-1} for the electrochemical characterization of oxides.

All solutions used in this work were prepared with 18 MΩ cm water produced by a reagent water system (Milli-Q SP, Japan), and all reagents not otherwise specified in this work were Merck, GR. In addition, the deposition baths and the 0.5 M H_2SO_4 solution used to study the electrochemical behavior of oxides were degassed with purified nitrogen gas before voltammetric measurements meanwhile nitrogen was passed over the solutions during the measurements. Temperature of the 0.5 M H_2SO_4 solution was maintained at 25 °C by means of a water thermostat (HAAKE DC3 and K20).

3. Results and discussion

3.1. Effects of storage time

In our previous work [7], the initial pH of the deposition baths has been demonstrated to strongly influence the rate (and probably the mechanisms) of $RuO_x \cdot nH_2O$ deposition. This effect was considered to be due to the chemical conversion of the dissolved $RuCl_3 \cdot aH_2O$ into the $Ru(OH)_\delta Cl_{3-\delta} \cdot cH_2O$ structure. This proposal was further verified by monitoring the variation of pH with the storage time of a $RuCl_3 \cdot aH_2O$ solution. Typical results for a 5 mM $RuCl_3 \cdot aH_2O$ solution are shown as curve 1 in Fig. 1b. In addition, results for the solution containing 5 mM $RuCl_3 \cdot aH_2O$ and 1 mM $IrCl_3 \cdot bH_2O$ are also shown as curve 2 in Fig. 1b. Note that pH of pure water should be neutral while a sharp decrease in pH was found when the chloride precursors were added into water (see Fig. 1a). Moreover, pH of both solutions decreased almost linearly with storage time (see Fig. 1b) when the storage time was longer than 6 h. These results demonstrate a chemical reaction between $RuCl_3 \cdot aH_2O$ ($IrCl_3 \cdot bH_2O$) and water molecules, which can be simply expressed as follows:

$$MCl_3 \cdot aH_2O \xrightarrow{H_2O} MCl_3 \cdot cH_2O \quad (1)$$

$$MCl_3 \cdot cH_2O + H_2O \rightarrow M(OH)_\delta Cl_{3-\delta} \cdot cH_2O + \delta H^+ + \delta Cl^- \quad (2)$$

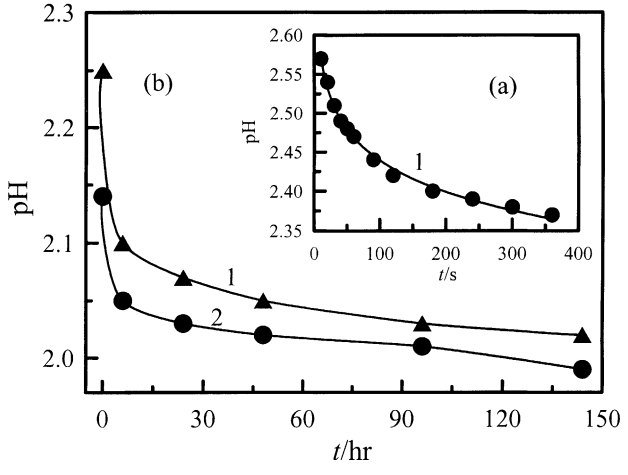

Fig. 1. (a) The initial 360 s of curve 1 in (b); and (b) pH against the storage time for a solution containing (1) 5 mM $RuCl_3 \cdot aH_2O$, (2) 5 mM $RuCl_3 \cdot aH_2O$ and 1 mM $IrCl_3 \cdot bH_2O$ at 25 °C.

where M is indicative of Ru or Ir atoms. Note that the chemical conversion from $MCl_3{\cdot}cH_2O$ into $M(OH)_\delta Cl_{3-\delta}{\cdot}cH_2O$ donates protons to the solution, resulting in a decrease in pH, which is similar to a sol–gel process [17]. From the decrease in pH for both solutions in Fig. 1, the total amount of coordinated chlorides replaced by hydroxyl- and/or oxy-groups can be theoretically calculated on the basis of Eq. (2). In addition, the number of coordinated chlorides (in average) replaced by hydroxyl- and/or oxy-groups (denoted as δ) for every $RuCl_3{\cdot}cH_2O$ molecule can be estimated by the following equation:

$$\delta = \frac{[H^+]_t - [H^+]_{t_0}}{[RuCl_3 \cdot aH_2O]} = \frac{[H^+]_t - 10^{-7}}{5 \times 10^{-3}} \quad (3)$$

where $[H^+]_t$, $[H^+]_{t_0}$, and $[RuCl_3{\cdot}aH_2O]$ represent the proton concentrations at storage time of t, and t_0, and the $RuCl_3{\cdot}aH_2O$ concentration, respectively. These results are shown in Table 1. Note that approximate 0.45 coordinated chloride was immediately replaced for every $RuCl_3{\cdot}aH_2O$ molecule when $RuCl_3{\cdot}aH_2O$ was dissolved in water. After storing for 6 h, about 1.52 coordinated chlorides were replaced for every $RuCl_3{\cdot}aH_2O$ molecule and then, δ increased almost linearly with the storage time. Also note that δ is not an integer, indicating that the number of coordinated chlorides replaced by the hydroxyl- and/or oxy-groups is not in a stoichiometric ratio. This leads to the speculation that certain amount of central metal atoms may share the replacing hydroxyl- and/or oxy-groups, implying the formation of aggregates consisting of chloro-oxy-hydroxyl-ruthenium species. This inference was further supported by the finding of a somewhat fogy solution (i.e. the formation of colloids) after the 5 mM $RuCl_3{\cdot}aH_2O$ solution was stored at 25 °C for 4 or more weeks. From the earlier results and discussion, the rate of coordinated chloride replacement should be very fast during the initial several hours (ca. from 0 to 6 h).

Similarly, the number of coordinated chlorides (in average) replaced by hydroxyl- and/or oxy-groups (denoted as ω) for every $RuCl_3{\cdot}aH_2O$ and $IrCl_3{\cdot}bH_2O$ molecule can be estimated by the following equation:

$$\omega = \frac{[H^+]_t - [H^+]_{t_0}}{[RuCl_3 \cdot aH_2O] + [IrCl_3 \cdot bH_2O]} = \frac{[H^+]_t - 10^{-7}}{6 \times 10^{-3}} \quad (4)$$

Table 1
Effects of storage time on the degree of chemical conversion for the dissolved metal-chloride precursors

	Storage time (h)					
	0	6	24	48	96	144
pH[a]	2.65	2.12	2.08	2.05	2.03	2.02
$[Cl^-]$ (mM)[a]	2.24	7.59	8.32	8.91	9.33	9.55
δ	0.45	1.52	1.66	1.78	1.87	1.91
pH[b]	2.32	2.06	2.03	2.01	2.00	1.99
$[Cl^-]$ (mM)[b]	4.79	8.71	9.33	9.77	10.0	10.23
ω	0.8	1.45	1.56	1.63	1.67	1.71
δ'	0.36	1.14	1.27	1.35	1.4	1.45

[a] For the 5 mM $RuCl_3{\cdot}aH_2O$ solution.
[b] For the 5 mM $RuCl_3{\cdot}aH_2O$ and 1 mM $IrCl_3{\cdot}bH_2O$ solution.

where $[IrCl_3{\cdot}bH_2O]$ represents the concentration of the dissolved $IrCl_3{\cdot}bH_2O$ precursor. These data are also shown in Table 1. A comparison of δ and ω reveals that the degree of coordinated chloride replacement for every $RuCl_3{\cdot}aH_2O$ molecule was depressed by the presence of $IrCl_3{\cdot}bH_2O$ with the exception when t was equal to 0 (i.e. $\delta = 0.45$ and $\omega = 0.8$ at $t \approx 0$). Since pure hydrous iridium oxide (i.e. $IrO_z{\cdot}kH_2O$) can not be deposited by cyclic voltammetry [3,8,16], the earlier phenomenon may be attributed to a very fast and over-replacement of the coordinated chlorides for $IrCl_3{\cdot}bH_2O$ (presumably the formation of $Ir(OH)_3{\cdot}dH_2O$). Based on this assumption, the number of coordinated chlorides (in average) replaced by hydroxyl- and/or oxy-groups (denoted as δ') for every $RuCl_3{\cdot}aH_2O$ molecule can be estimated by the following equation:

$$\delta' = \frac{[H^+]_t - [H^+]_{t_0} - 3[IrCl_3 \cdot bH_2O]}{[RuCl_3 \cdot aH_2O]} = \frac{[H^+]_t - 10^{-7} - 3 \times 10^{-3}}{5 \times 10^{-3}} \quad (5)$$

These data are also shown in the last row of Table 1. Note that at any storage time, δ' is obviously smaller than δ, indicating the inhibition of the coordinated chloride replacement of $RuCl_3{\cdot}aH_2O$ due to an over-replacement of the coordinated chlorides of $IrCl_3{\cdot}bH_2O$.

Since pH of the precursor solutions varied with storage time, effects of this variable on the rate of oxide deposition and the electrochemical properties of hydrous oxide films were investigated. Typical cyclic voltammograms for oxide deposition measured in two solutions containing 5 mM $RuCl_3{\cdot}aH_2O$ and 0.1 M KCl with their storage time of 20 min (including heating from room temperature to 50 °C and oxygen degassing) and 144 h are shown in Fig. 2a and b, respectively. Note that the initial pH of both solutions was adjusted to 2.5 before the voltammetric deposition since the rate of $RuO_x{\cdot}nH_2O$ deposition reached a maximum at this initial pH [7]. From a comparison of Fig. 2a and b, two features have to be noted. First, the redox shoulders, C_1/A_1, were still found in Fig. 2a although this redox reaction seemed to be more hysteretic with the deposition cycles. In Fig. 2b, these redox shoulders were obscurely found in the initial 30 cycles and disappeared in the following cycles. It is worthy noting that only peaks C_2/A_2 were observed on the CV diagrams of the $RuO_x{\cdot}nH_2O$ deposition when the initial pH of baths (storage time $\approx$ 20 min) was $\geq$3.0 [7]. Hence, the disappearance of C_1/A_1 is expected to indicate an over-replacement of the coordinated chlorides (i.e. the formation of an OH-rich Ru species). The formation of OH-rich Ru species should depress the rate of $RuO_x{\cdot}nH_2O$ deposition since it reached a maximum at an initial pH of 2.5 [7]. Second, the electrochemical reversibility of the redox reaction corresponding to peaks C_2/A_2 in Fig. 2a is better than that in Fig. 2b. This result indicates that the electrochemical reversibility of oxide deposition is significantly depressed by increasing

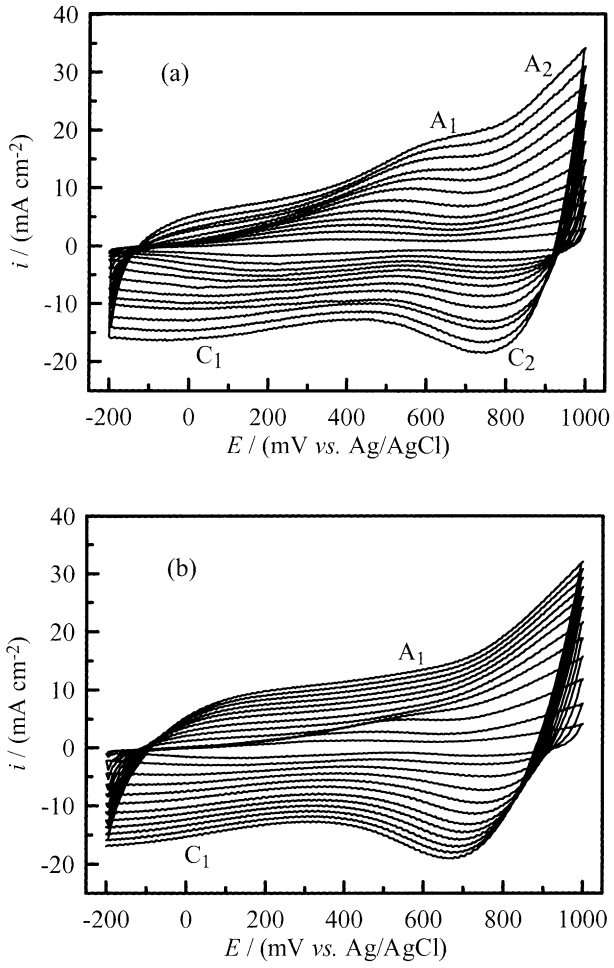

Fig. 2. Cyclic voltammograms of $RuO_x{\cdot}nH_2O$ deposition at 50 mV s^{-1} and 50 °C in a 5 mM $RuCl_3{\cdot}aH_2O$ and 0.1 M KCl bath with the storage time of (a) 20 min; and (b) 144 h.

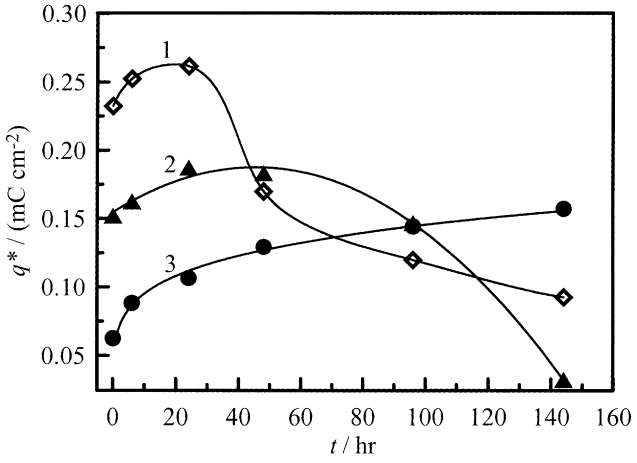

Fig. 3. Effects of storage time on the voltammetric charges of $RuO_x{\cdot}nH_2O$ films deposited from a 5 mM $RuCl_3{\cdot}aH_2O$ and 0.1 M KCl solution with initial pH of (1) 2.5, (2) 2.15 and (3) of $(Ru + Ir)O_y{\cdot}mH_2O$ films from a bath containing 5 mM $RuCl_3{\cdot}aH_2O$, 1 mM $IrCl_3{\cdot}bH_2O$ and 0.1 M KCl with initial pH of 2.15.

the storage time, probably due to the chemical conversion from $RuCl_3{\cdot}aH_2O$ into $Ru(OH)_\delta Cl_{3-\delta}{\cdot}cH_2O$. The above phenomena imply that the redox transitions during the oxide deposition became more hysteresis when an OH-rich structure of the dissolved ruthenium species, gradually converted from the Cl-rich structure, was formed in the deposition bath.

The effects of storage time on the rate of oxide deposition were compared through means of their voltammetric charges from the CVs measured in an inert electrolyte. Typical results for the $RuO_x{\cdot}nH_2O$ films deposited from the 5 mM $RuCl_3{\cdot}aH_2O$ and 0.1 M KCl solutions with their initial pH of 2.5 and 2.15 are shown as curves 1 and 2 in Fig. 3, respectively. In addition, the effects of storage time on the voltammetric charges of $(Ru + Ir)O_y{\cdot}mH_2O$ films deposited from a bath containing 5 mM $RuCl_3{\cdot}aH_2O$, 1 mM $IrCl_3{\cdot}bH_2O$, and 0.1 M KCl with its initial pH of 2.15 are also shown as curve 3 in Fig. 3. From a comparison of curves 1 and 2, several important features have to be mentioned. First, voltammetric charges reached a maximum at the storage time of ca. 24 h on curve 1 (i.e. the initial case pH = 2.5) while they reached a maximum at the storage time of ca. 40 h on curve 2 (i.e. the initial case pH = 2.15). Second, the maximal voltammetric charge (0.26 C cm^{-2}) fabricated from the former solution was much larger than that (0.19 C cm^{-2}) prepared from the latter solution. Third, on curve 1, the voltammetric charge decreased sharply when it just passed through the maximum and then, a gradual decrease in voltammetric charges was found with the storage time. However, an opposite trend was found on curve 2. The above difference indicates that (i) the formation of an OH-rich Ru precursor renders a decrease in the deposition rate of $RuO_x{\cdot}nH_2O$ and (ii) the initial pH of deposition solutions also exhibits significant influences on the deposition rate.

On curve 3, voltammetric charges of $(Ru + Ir)O_y{\cdot}mH_2O$ films increased more quickly with the storage time during the initial 8 h and then increased almost linearly in the following storage period (i.e. 8–144 h). In addition, from an examination of Fig. 3, the voltammetric charges of binary oxide were obviously smaller than those of $RuO_x{\cdot}nH_2O$ films obtained in the baths with initial pH of 2.15 and 2.5 when the storage time was shorter than 48 h. However, an opposite result was found when the storage time was longer than ca. 96 h. The former result reveals that the rate of oxide deposition was significantly depressed by the presence of $IrCl_3{\cdot}bH_2O$ in the deposition solution, which has also been found previously [3,8,16]. The latter result can be explained by the inhibition of an over-replacement of the coordinated chlorides for $RuCl_3{\cdot}aH_2O$ due to the presence of $IrCl_3{\cdot}bH_2O$ (see Table 1) since the over-replacement of coordinated chlorides of the dissolved precursors inhibited the oxide deposition.

3.2. Effects of preheating

Since the conversion of $RuCl_3{\cdot}aH_2O$ into $Ru(OH)_\delta Cl_{3-\delta}{\cdot}cH_2O$ is a chemical reaction, this reaction should be

Table 2
Effects of preheating for 20 min on the degree of chemical conversion for the dissolved metal-chloride precursors and voltammetric charges of $RuO_x{\cdot}nH_2O$ and $(Ru + Ir)O_y{\cdot}mH_2O$ deposits measured in 0.5 M H_2SO_4 at 20 mV s^{-1}

	Preheating temperature (°C)		
	25	60	80
pH[a]	2.65	1.95	1.87
$[Cl^-]$ (mM)[a]	2.24	11.22	13.49
δ	0.45	2.24	2.7
q^* (mC cm^{-2})[a]	232.2	72.0	41.6
Loss in q^* (%)[a]	–	69.05	75.13
pH[b]	2.32	1.89	1.82
$[Cl^-]$ (mM)[b]	4.79	12.88	15.14
ω	0.8	2.15	2.52
δ'	0.35	1.98	2.43
q^* (mC cm^{-2})[b]	186.0	99.7	76.4
Loss in q^* (%)[b]	–	46.4	58.9

[a] For the 5 mM $RuCl_3{\cdot}aH_2O$ solution.
[b] For the 5 mM $RuCl_3{\cdot}aH_2O$ and 1 mM $IrCl_3{\cdot}bH_2O$ solution.

accelerated by preheating the deposition solution. Typical results of q^* for $RuO_x{\cdot}nH_2O$ and $(Ru + Ir)O_y{\cdot}mH_2O$ deposits, measured in 0.5 M H_2SO_4 at 20 mV s^{-1}, against preheating temperature are shown in Table 2. Note that the $RuCl_3{\cdot}aH_2O$ and $IrCl_3{\cdot}bH_2O$ solutions were preheated individually for 20 min, then added KCl to reach the specified concentration (i.e. 5 mM $RuCl_3{\cdot}aH_2O$, 1 mM $IrCl_3{\cdot}bH_2O$, and 0.1 M KCl), and finally adjusted to the initial pH. In addition, the final pH values of the preheating solutions containing 5 mM $RuCl_3{\cdot}aH_2O$ and 5 mM $RuCl_3{\cdot}aH_2O$ and 1 mM $IrCl_3{\cdot}bH_2O$ are also shown in this table in order to calculate the number of coordinated chlorides replaced by hydroxyl- and/or oxy-groups (see δ, ω and δ'). From an examination of q^* data, the loading of both $RuO_x{\cdot}nH_2O$ and $(Ru + Ir)O_y{\cdot}mH_2O$ deposits was obviously lower than that of their unheated counterparts, indicating an inhibition of oxide deposition due to preheating the precursors. This phenomenon is predicable since δ is approximately equal to 2.7 for the 5 mM $RuCl_3{\cdot}aH_2O$ preheated at 80 °C for 20 min, indicating a highly over-replacement of the coordinated chlorides. From the earlier results and discussion, it is reasonable to believe that an over-replacement of the coordinated chlorides of the dissolved precursors obviously inhibited the oxide deposition.

In previous section, the rate of $(Ru + Ir)O_y{\cdot}mH_2O$ deposition was gradually promoted with increasing the storage time while it was obviously depressed by preheating. Hence, conflict effects of the chloride replacement on the rate of $(Ru + Ir)O_y{\cdot}mH_2O$ deposition seem to be found. However, a comparison of the δ' values in Table 1 (i.e. 1.45) with those in Table 2 (i.e. 1.98 and 2.43) reveals that the number of coordinated chlorides replaced by hydroxyl- and/or oxy-groups for every $RuCl_3{\cdot}aH_2O$ molecule after preheating is much larger than that with a storage time of 144 h. The effects of chemical conversion of $RuCl_3{\cdot}aH_2O$ on the rate of oxide deposition for the earlier two cases are probably different since a suitable replacement of the coordinated chloride of $RuCl_3{\cdot}aH_2O$ is expected to promote the rate of oxide deposition. It is worthy noting that a comparison of q^* data between $RuO_x{\cdot}nH_2O$ and $(Ru + Ir)O_y{\cdot}mH_2O$ deposits reveals the larger loss in q^* due to preheating for the former oxide. Therefore, the presence of $IrCl_3{\cdot}bH_2O$ depressed the over-replacement of coordinated chlorides of $RuCl_3{\cdot}aH_2O$, providing a positive effect on the rate of $(Ru + Ir)O_y{\cdot}mH_2O$ deposition. This inference was further supported by the significant difference between δ and δ' in Table 2.

3.3. Effects of initial pH on the rate of binary Ru–Ir oxide deposition

In our previous paper [7], the rate (and probably the mechanisms) of $RuO_x{\cdot}nH_2O$ deposition onto the titanium substrate was strongly affected by the initial pH of the deposition baths. Moreover, the deposition of $(Ru+Ir)O_y{\cdot}mH_2O$ was obviously inhibited by the presence of $IrCl_3{\cdot}bH_2O$ in the deposition solutions although pseudocapacitance of the mixed oxides reached a maximum at $[IrCl_3{\cdot}bH_2O]{:}[RuCl_3 \cdot aH_2O] = 1{:}5$ [3]. Therefore, the effects of initial pH of the deposition baths on the deposition rate and the electrochemical properties of $(Ru + Ir)O_y{\cdot}mH_2O$ films were also studied in this work. Typical cyclic voltammograms of the $(Ru + Ir)O_y{\cdot}mH_2O$ deposition from a solution containing 5 mM $RuCl_3{\cdot}aH_2O$, 1 mM $IrCl_3{\cdot}bH_2O$, and 0.1 M KCl with the initial pH of 2.15 and storage time of 144 h are shown in Fig. 4.

In general, these deposition curves are very similar in shape to those of $(Ru + Ir)O_y{\cdot}mH_2O$ deposited from the same plating bath with storage time ≈0 (20 min) [3]. For example, two pairs of redox peaks (labeled as C_1/A_1 and C_2/A_2, respectively) are found although peak C_1 is relatively smoother. In addition, passive behavior was observed between −200 and 100 mV on the positive sweeps at cycle

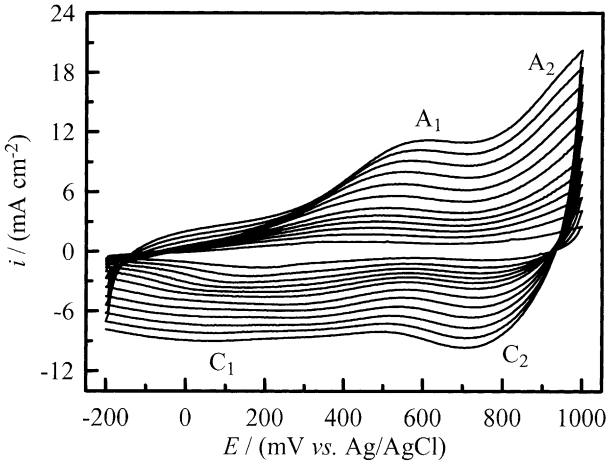

Fig. 4. Cyclic voltammograms of $(Ru + Ir)O_y{\cdot}mH_2O$ deposition at 50 mV s^{-1} and 50 °C in a solution containing 5 mM $RuCl_3{\cdot}aH_2O$, 1 mM $IrCl_3{\cdot}bH_2O$ and 0.1 M KCl with initial pH of 2.15 and a storage time of 144 h.

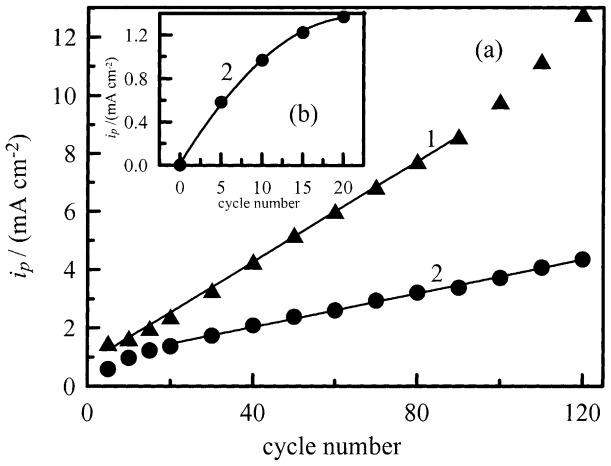

Fig. 5. (a) i_p of A_1 for $(Ru + Ir)O_y{\cdot}mH_2O$ deposition against the cycle number of CVs from a plating bath containing 5 mM $RuCl_3{\cdot}aH_2O$, 1 mM $IrCl_3{\cdot}bH_2O$, and 0.1 M KCl with initial pH of (1) 2.15, (2) 2.5; and (b) the initial 20 cycles of curve 1 in (a).

number below 100 and voltammetric currents were approximately potential-dependent and increased with the cycle number of CV. Since these deposition curves were very similar to those of $RuO_x{\cdot}nH_2O$ deposition [4] and since an OH-rich Ir species was expected to form in the deposition solution (see the Section 1), the kinetics of binary oxide deposition should be dominated by the mechanism of $RuO_x{\cdot}nH_2O$ deposition.

In our previous work [3,4,7,8], i_p of A_1 was indicative of the relative loading and pseudocapacitance of the oxides fabricated from the same deposition solutions. In addition, the slope of i_p of A_1 against the cycle number of CV for oxide deposition showed the deposition rate. Thus, i_p of A_1 for $(Ru + Ir)O_y{\cdot}mH_2O$ deposition against the cycle number of CVs was examined. Typical results for the plating baths containing 5 mM $RuCl_3{\cdot}aH_2O$, 1 mM $IrCl_3{\cdot}bH_2O$, and 0.1 M KCl with the storage time of 144 h and their initial pH of 2.15 and 2.5 are respectively shown as curves 1 and 2 in Fig. 5a. In general, the peak current is directly proportional to the number of deposition cycles in both cases, as evidenced by the two linear lines in Fig. 5a. The slope of i_p against cycle number, however, is much lower for the solution with a higher initial pH, indicating a relatively slow rate of deposition. From an examination of Fig. 5, two features have to be discussed. First, in both solutions, the induced period of the oxide deposition was not found, especially for the oxide deposited from the bath with the initial pH of 2.5 (see Fig. 5b). Second, there were two linear regions on curve 1, suggesting a more rapid rate of $(Ru + Ir)O_y{\cdot}mH_2O$ deposition at the cycle number of CVs above 90. In fact, a change in growth rate for the $RuO_x{\cdot}nH_2O$ deposition has also been found when the deposition solution was kept at 65 °C (above 60 cycle) [7]. This phenomenon was attributed to the formation of a suitable $Ru(OH)_\delta Cl_{3-\delta}{\cdot}cH_2O$ structure (due to a suitable replacement of the coordinated chlorides), promoting the rate of oxide deposition. Note that a longer storage time increased the degree of chemical conversion of $RuCl_3{\cdot}aH_2O$ into $Ru(OH)_\delta Cl_{3-\delta}{\cdot}cH_2O$, which could be accelerated by heating the solutions. In addition, the deposition of both $RuO_x{\cdot}nH_2O$ and $(Ru + Ir)O_y{\cdot}mH_2O$ films was usually carried out at a higher temperature (e.g. 50 °C). Thus, the chemical conversion of $RuCl_3{\cdot}aH_2O$ into $Ru(OH)_\delta Cl_{3-\delta}{\cdot}cH_2O$ and the deposition of hydrous oxides should occur simultaneously during the CV deposition process. Based on the earlier discussion, the structure of $RuCl_3{\cdot}aH_2O$ in the deposition baths should vary with the CV cycles of oxide deposition (i.e. the deposition time). Since the rate of $RuO_x{\cdot}nH_2O$ and $(Ru + Ir)O_y{\cdot}mH_2O$ deposition could be promoted by a suitable replacement of the coordinated chlorides of $RuCl_3{\cdot}aH_2O$, a more rapid rate of $RuO_x{\cdot}nH_2O$ or $(Ru + Ir)O_y{\cdot}mH_2O$ deposition should be obtained when the CVs of deposition were above certain cycles.

3.4. Pseudocapacitance evaluation

Hydrous oxides (e.g. $RuO_x{\cdot}nH_2O$ and $(Ru + Ir)O_y{\cdot}mH_2O$) have been recognized to be one of the most promising materials applicable for the electrochemical supercapacitors since these electroactive materials prosecuted reversible redox transitions between various oxidation states in the potential range of water decomposition [1–4,7–9,12,13]. The capacitance mainly coming from the fast faradaic redox transitions of electroactive materials is called pseudocapacitance [1–9], which is very different in electrochemical characteristics from the double-layer capacitance. For $RuO_x{\cdot}nH_2O$ and $(Ru + Ir)O_y{\cdot}mH_2O$, pseudocapacitance should mainly come from the M(III)/M(II), M(IV)/M(III) and M(VI)/M(IV) transitions [3,4,14,15,18], where M indicates both Ru and Ir. In addition, the number of electroactive oxycations involving in the redox transitions can be efficiently evaluated by means of q^* [3,4,14,15,18], which is integrated from a cyclic voltammogram measured in an inert electrolyte (e.g. 0.5 M H_2SO_4). Therefore, pseudocapacitance of hydrous oxides can be estimated from q^*. Note that the performance of an EC supercapacitor is predominantly determined by the electrochemical reversibility of the redox transitions at/within the electroactive materials. This important property can also be efficiently examined by cyclic voltammetry [3–8].

Typical CV diagrams measured in 0.5 M H_2SO_4 for the oxide-coated electrodes deposited from the plating solutions containing 5 mM $RuCl_3{\cdot}aH_2O$ and 1 mM $IrCl_3{\cdot}bH_2O$ with initial pH values of 1.9, 2.15, 2.35, 2.5 are, respectively, shown as curves 1–4 in Fig. 6. On these curves, there are two pairs of symmetric redox peaks in the potential regions from 100 to 700 mV and 700 to 1150 mV, indicating good reversibility of the redox couples at/within the hydrous oxides. The former and latter peaks are likely attributed to the redox couples of Ru(IV)/Ru(III)/Ru(II) and Ru(VI)/Ru(IV), respectively [18]. In addition, the shape of these *i–E* curves is similar to each other, which are very similar in shape to

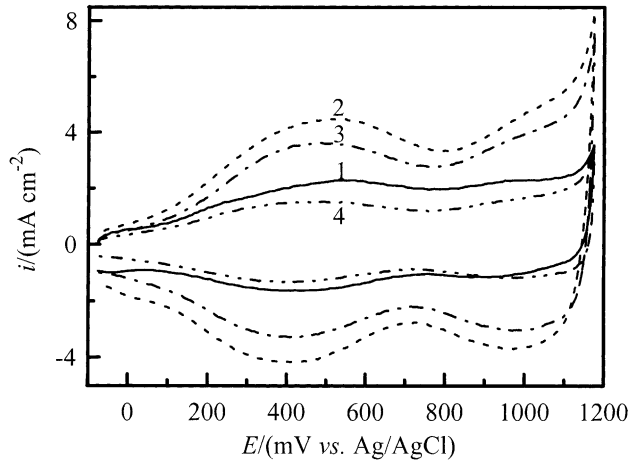

Fig. 6. Cyclic voltammograms of $(Ru + Ir)O_y{\cdot}mH_2O$ electrodes in 0.5 M H_2SO_4; the oxide-coated electrodes were deposited from the plating solutions containing 5 mM $RuCl_3{\cdot}aH_2O$, 1 mM $IrCl_3{\cdot}bH_2O$ and 0.1 M KCl with initial pH of (1) 1.9, (2) 2.15, (3) 2.35, and (4) 2.5.

those of $RuO_x{\cdot}nH_2O$, demonstrating that $RuO_x{\cdot}nH_2O$ is the main electroactive species within the binary hydrous oxides.

The effect of initial pH of the plating baths on q^* of $(Ru + Ir)O_y{\cdot}mH_2O$ is shown in Fig. 7a. Since a higher voltammetric charge of a hydrous oxide-coated electrode should result from a higher loading and/or a higher degree of utilization of oxides, the specific capacitance (C_S) (based on unit mass) of various $(Ru + Ir)O_y{\cdot}mH_2O$ deposits is thus employed to distinguish these two effects. Typical result of C_S against the initial pH of electroplating baths is shown in Fig. 7b. Note in Fig. 7a that with increasing the initial pH values of plating baths from 1.9 to 2.6, voltammetric charges reached a maximum at an initial pH of ca. 2.15. In addition, the loading of $(Ru + Ir)O_y{\cdot}mH_2O$ deposits also reached a maximum at this pH value. These results reveal that the rate of oxide deposition is significantly influenced by the initial pH of the plating baths. This effect is reasonably attributed to the strong effect of the initial pH on the degree of chemical conversion of $RuCl_3{\cdot}aH_2O$. Also note that in our previous work [7], the rate of $RuO_x{\cdot}nH_2O$ deposition reached a maximum when the initial pH was equal to ca. 2.5. However, the loading of $(Ru + Ir)O_y{\cdot}mH_2O$ deposits decreased very sharply when the initial pH of plating baths was above 2.35, indicating the obvious inhibition of oxide deposition due to the presence of $IrCl_3{\cdot}xH_2O$. Thus, there very likely exists a compromise between the enhancement of oxide deposition due to the initial pH influencing the degree of chemical conversion for $RuCl_3{\cdot}aH_2O$ and the inhibition of $(Ru + Ir)O_y{\cdot}mH_2O$ deposition because of the presence of $IrCl_3{\cdot}bH_2O$ (probably $Ir(OH)_3{\cdot}dH_2O$). This compromise effect may result in the existence of a maximum for the loading and q^* of $(Ru + Ir)O_y{\cdot}mH_2O$ deposits when the initial pH value of the deposition bath is equal to 2.15.

The pseudocapacitance of these hydrous oxides was calculated on the basis of the following equations [3–8]:

$$C_{q^*} = \frac{\text{voltammetric charge}}{\text{voltage range}} = \frac{q^*}{\Delta V} \tag{6}$$

$$C_S = \frac{C_{q^*}}{\text{loading of electrodes}} \tag{7}$$

where C_{q^*} and C_S are respectively indicative of pseudocapacitance and specific capacitance of each electrode. Note that data of the specific capacitance, shown in Fig. 7b, for the $(Ru + Ir)O_y{\cdot}mH_2O$ films deposited from the solutions with initial pH >2.35 were not precise because their loading is too small to measure accurately. In Fig. 7b, the specific capacitance of $(Ru + Ir)O_y{\cdot}mH_2O$ gradually increased from ca. 220 to 380 F g^{-1} with the continuous increase in initial pH of the deposition baths. This result indicates that the electrochemical and textural properties of $(Ru + Ir)O_y{\cdot}mH_2O$ should be significantly influenced by the initial pH of the deposition solutions. In our previous work [3], the intercalation of $IrO_z{\cdot}kH_2O$ was found to enhance the utilization

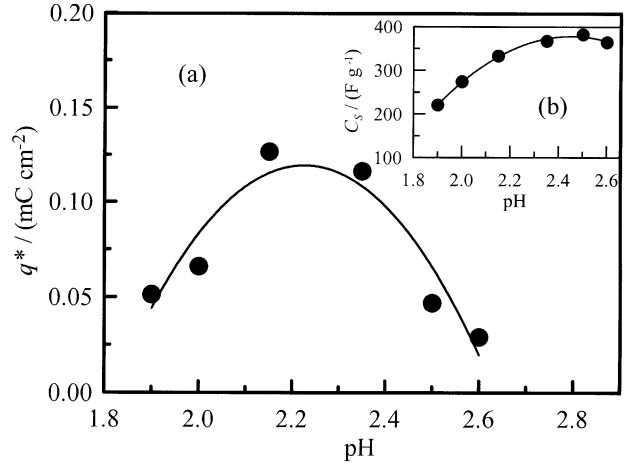

Fig. 7. (a) Voltammetric charges, q^*; and (b) specific capacitance, C_S, of the $(Ru + Ir)O_y{\cdot}mH_2O$ electrodes against the initial pH of deposition baths.

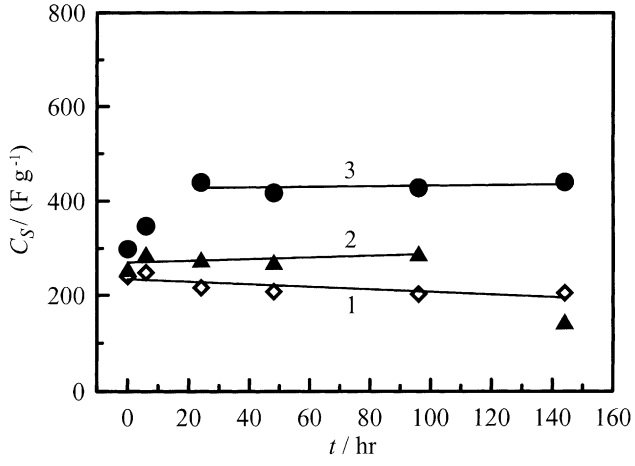

Fig. 8. Specific capacitance against the storage time of deposition baths for (1) $RuO_x{\cdot}nH_2O$ prepared at initial pH of 2.5, (2) $RuO_x{\cdot}nH_2O$ prepared at initial pH of 2.15, and (3) $(Ru + Ir)O_y{\cdot}mH_2O$ prepared at initial pH of 2.15.

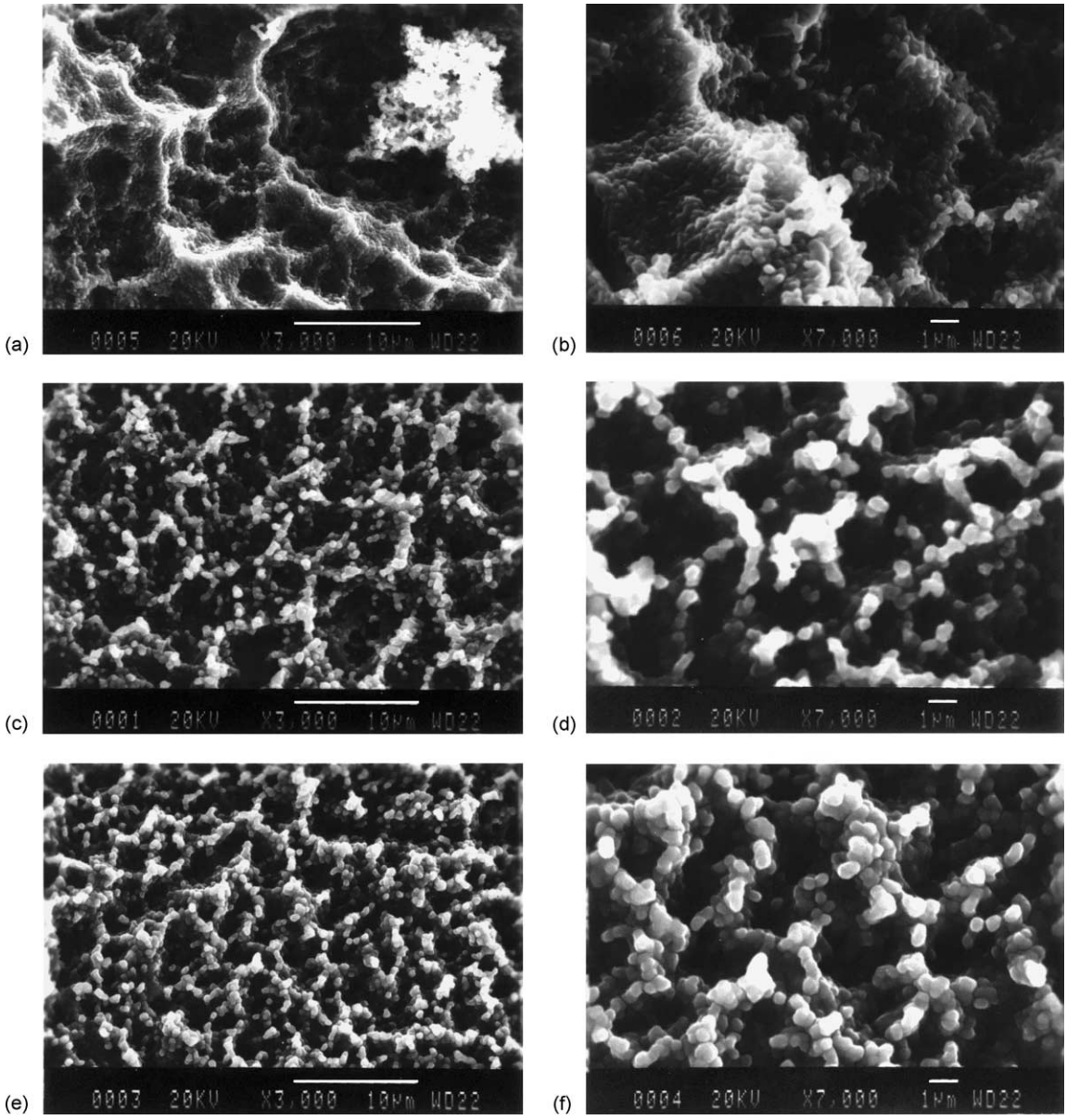

Fig. 9. SEM photographs of the deposits grown from the baths with ($RuCl_3{\cdot}aH_2O$, $IrCl_3{\cdot}bH_2O$) concentrations equal to (a) (5, 0) mM and initial pH of 2.15; (c) (5, 1) mM and initial pH of 2.15; (e) (5, 1) mM and initial pH of 1.9, respectively (3000×); and (b) (5, 0) mM and initial pH of 2.15; (d) (5, 1) mM and initial pH of 2.15; (f) (5, 1) mM and initial pH of 1.9, respectively (7000×).

of $RuO_x{\cdot}nH_2O$, due to an increase in non-stoichiometric site. The earlier results, a change in specific capacitance for $(Ru + Ir)O_y{\cdot}mH_2O$, may be resulted from a combination of (i) different degrees of intercalation and/or dispersion of $IrO_z{\cdot}kH_2O$ within the oxide matrix; and/or (ii) different microstructures (e.g. different surface area/volume ratios).

In order to gain a further understanding of the earlier phenomena, the effects of storage time on the specific capacitance of the following oxides: $RuO_x{\cdot}nH_2O$ prepared at initial pH of 2.5; $RuO_x{\cdot}nH_2O$ prepared at initial pH of 2.15; and $(Ru + Ir)O_y{\cdot}mH_2O$ prepared at initial pH of 2.15, were examined. These results are respectively shown as curves 1–3 in Fig. 8. On curve 1, C_S is approximately constant (≈200 F g^{-1}) in the whole duration of storage time. On curve 2, similar phenomenon is found but the constant specific capacitance is close to 285 F g^{-1}. The above difference in specific capacitance for $RuO_x{\cdot}nH_2O$ supports the inference that the microstructure (e.g. the surface area/volume ratio) of oxides is significantly influenced by the initial pH of the deposition baths. On curve 3, C_S increases obviously from ca. 300 to 400 F g^{-1} during the initial 24 h while it keeps almost constant in the following 120 h. This trend on curve 3 is very similar to the q^* data of the same series of electrodes. A comparison of curves 1–3 reveals that the utilization of $RuO_x{\cdot}nH_2O$ is considerably enhanced by the presence of $IrO_z{\cdot}kH_2O$, probably due to an increase in

non-stoichiometric sites and/or a change in microstructure, resulting in the obvious increase in specific capacitance of the binary oxides.

3.5. Scanning electron microscopic photographs

The earlier results and discussion suggest that the change in specific capacitance of $RuO_x{\cdot}nH_2O$ and $(Ru + Ir)O_y{\cdot}mH_2O$ deposits, prepared at different initial pH, can be linked to their different microstructures (e.g. the surface area/volume ratio). In order to gain an understanding of this relationship, scanning electron microscopy is used to examine the microstructure of the following films: $RuO_x{\cdot}nH_2O$ prepared at initial pH of 2.15; $(Ru + Ir)O_y{\cdot}mH_2O$ prepared at initial pH of 2.15; and $(Ru + Ir)O_y{\cdot}mH_2O$ prepared at initial pH of 1.9. These results are shown in Fig. 9. In Fig. 9a, the uneven $RuO_x{\cdot}nH_2O$ film, probably due to the porous nature of the titanium substrate, is relatively compact. The relatively low degree of utilization for the electroactive Ru species may be due to this more compact nature. On the other hand, the average size of the spherical $RuO_x{\cdot}nH_2O$ particles is ca. 0.3 μm (see Fig. 9b). Thus, if the $RuO_x{\cdot}nH_2O$ film has a hyper-extended microstructure, the utilization of the electroactive species must be highly promoted. In Fig. 9c, the morphology of the binary oxide film is very porous with many open holes, which favors the penetration of electrolytes (e.g. proton) into the oxide matrix. However, the average size of the spherical $(Ru + Ir)O_y{\cdot}mH_2O$ particles is about 0.4–0.5 μm (see Fig. 9d). A comparison between Fig. 9a and c demonstrates that the porosity (i.e. surface area) of a $RuO_x{\cdot}nH_2O$ deposit is sharply increased by the intercalation of $IrO_z{\cdot}kH_2O$. Accordingly, the utilization of $RuO_x{\cdot}nH_2O$ is promoted by the presence of $IrO_z{\cdot}kH_2O$. The change in microstructure indicates the influence of $IrCl_3{\cdot}bH_2O$ (probably $Ir(OH)_3{\cdot}dH_2O$) on the mechanism of binary oxide deposition although the voltammetric curves of $(Ru + Ir)O_y{\cdot}mH_2O$ deposition remains the key features of $RuO_x{\cdot}nH_2O$ deposition. A comparison of Fig. 9c and e reveals that morphologies of the $(Ru + Ir)O_y{\cdot}mH_2O$ films prepared at different initial pH are very similar to each other while the open pores distributed on the former deposit (i.e. prepared at initial pH of 2.15) is larger than the latter (i.e. prepared at initial pH of 1.9). Note that the average size of the spherical $(Ru + Ir)O_x{\cdot}nH_2O$ particles prepared at initial pH of 1.9 (see Fig. 9f) is somewhat larger than those prepared at initial pH of 2.15. Thus, the decrease in initial pH of the deposition baths causes the increase in particle size and the decrease in porosity (i.e. a decrease in surface area). Hence, a lower utilization of $RuO_x{\cdot}nH_2O$ was found in this case.

4. Conclusions

The rate of $(Ru + Ir)O_y{\cdot}mH_2O$ and $RuO_x{\cdot}nH_2O$ deposition was predominantly determined by the structure of the dissolved ruthenium and iridium precursors and the initial pH of the deposition baths. The structures of these precursors could be effectively controlled by preheating, changing the storage time and adjusting initial pH of the deposition baths. The intercalation of $IrO_z{\cdot}kH_2O$ and the initial pH of the deposition baths were found to significantly influence the microstructures of oxides, resulting in the different degrees of utilization of the electroactive species although the deposition of $(Ru + Ir)O_y{\cdot}mH_2O$ was significantly depressed by the presence of $IrCl_3{\cdot}bH_2O$ (probably $Ir(OH)_3{\cdot}dH_2O$).

Acknowledgements

The financial support of this work, by the National Science Council of the Republic of China under contract no. NSC 90-2214-E-194-007, is gratefully acknowledged.

References

[1] B.E. Conway, Electrochemical Supercapacitors, Kluwer Academic Publishers/Plenum Press, New York, 1999.
[2] S. Sarangapani, B.V. Tilak, C.-P. Chen, J. Electrochem. Soc. 143 (1996) 3791.
[3] C.-C. Hu, K.-H. Chang, Electrochim. Acta 45 (2000) 2685.
[4] C.-C. Hu, Y.-H. Huang, J. Electrochem. Soc. 146 (1999) 2465.
[5] C.-C. Hu, C.-H. Chu, Mat. Chem. Phys. 65 (2000) 329.
[6] C.-C. Hu, C.-H. Chu, J. Electroanal. Chem. 503 (1-2) (2001) 105.
[7] C.-C. Hu, Y.-H. Huang, Electrochim. Acta 46 (2001) 3431.
[8] C.-C. Hu, Y.-H. Huang, K.-H. Chang, J. Power Sources 108 (2002) 117.
[9] M. Ramani, B.S. Haran, R.E. White, B.N. Popov, J. Electrochem. Soc. 148 (2001) A374.
[10] M. Ishikawa, M. Morita, M. Ihara, Y. Matsuda, J. Electrochem. Soc. 141 (1994) 1730.
[11] G.L. Bullard, H.B. Sierra-Alcazar, H.L. Lee, J.L. Morris, IEEE Trans. Magnet. 25 (1989) 102.
[12] Y. Takasu, T. Nakamura, H. Ohkawauchi, Y. Murakami, J. Electrochem. Soc. 144 (1997) 2601.
[13] J.P. Zheng, P.-J. Cygon, T.R. Jow, J. Electrochem. Soc. 142 (1995) 2699.
[14] S. Trasatti, Electrochim. Acta 36 (1991) 225.
[15] S. Ardizzone, G. Fregonara, S. Trasatti, Electrochim. Acta 35 (1990) 263.
[16] C.-C. Hu, Y.-H. Huang, in: V.I. Birss, N. Oyama (Eds.), Proceedings of the Electrochemical Society on Molecular Functions of Electroactive Thin Films, PV 98-26, The Electrochemical Society, Inc., NJ, 1999, p. 144.
[17] J.P. Zheng, Electrochem. Solid State Lett. 2 (1999) 359.
[18] T.-C. Wen, C.-C. Hu, J. Electrochem. Soc. 139 (1992) 2158.